

## Subshell stopping power of the elements for protons in the Born approximation

E. J. McGuire

*Sandia National Laboratories, Albuquerque, New Mexico 87185*

(Received 23 March 1981; revised manuscript received 19 April 1982)

The generalized oscillator-strength formulation of the Born approximation was used to generate a large sample of subshell excitation and ionization generalized oscillator strengths across the periodic table. These were used to calculate the excitation and ionization contributions to the proton stopping power by individual subshells. The subshell ionization stopping powers are expressed in scaled form, depending on the subshell ionization energy. Detailed comparison of the calculated total proton stopping power is in good agreement with experiment across the periodic table. Detailed calculations show the importance of outer-shell ionization and excitation to the total stopping power for protons with energy less than 10 MeV.

## I. INTRODUCTION

The modeling of proton energy deposition in pellet fusion targets requires accurate (better than a factor of 2) stopping powers for ionized high- $Z$  materials. Nardi *et al.*<sup>1</sup> have shown that for gold target at a temperature of 1 keV energy deposition in the plasma dominates energy deposition in the bound electrons; consequently, a simple model for the latter should suffice. However, below temperatures of 200 eV, for solid densities and lower, deposition in the bound electrons in high- $Z$  elements should be dominant.<sup>2</sup> Further, while energy deposited via ionization in ions is local, energy deposited via excitation may be radiated away, inhibiting the achievement of high temperatures. Hahn<sup>3</sup> has suggested that for high- $Z$  materials the excitation cross section dominates the ionization cross section with increasing degrees of ionization.

While there are alternative approaches to the calculation of stopping power at low<sup>4,5</sup> and high energy,<sup>6</sup> in practice their use involves experimental parameters (although recently<sup>7</sup> fully theoretical treatments have begun to appear). There is no experimental information on the stopping power of ions for protons. Further, these theories are not designed to separate excitation and ionization contributions to the stopping power. An alternative approach, adopted here, is to calculate the contribution to the stopping power of excitation and ionization of each atomic subshell. To reduce the volume of computation, scaling laws are sought on a subshell basis. If subshell scaling laws exist, they should emerge from calculations on a sample of subshells. Using the generalized oscillator-strength formulation of the Born approximation,<sup>6</sup> I have

shown that subshell scaling laws can be found for electron<sup>8</sup> and proton<sup>9</sup> ionization. Here I show that subshell scaling laws can be found for the ionization contribution to stopping power. As yet subshell scaling laws for the excitation contribution to stopping power have not been found. In comparing calculated stopping power with experiment, explicit calculations of excitation stopping power are used. Explicit excitation calculations typically require an order of magnitude less computer time than ionization calculations. As mentioned in earlier articles,<sup>8,9</sup> the scaled subshell ionization stopping power can be viewed as merely a device to present a large body of calculations in simplified form. However, the scaling hypothesis is broader in intent, as the scaled subshell ionization stopping powers are used in determining the stopping power of ions. In the following paper<sup>10</sup> a detailed comparison is made of the stopping power calculated with the scaled subshell results and calculated directly.

The calculations presented here treat only the contribution to stopping power of inelastic collisions (excitation and ionization) between protons and atoms or ions. For plasmas, additional energy-loss mechanisms exist, e.g., energy loss to the free electrons. Mehlhorn<sup>2</sup> has presented a comprehensive model including all important energy-loss mechanisms. It was felt that the contribution of inelastic-proton—high- $Z$ -ion collisions was the least reliable portion of the model, and to remedy this these calculations were undertaken.

In Sec. II the details of the stopping-power calculations and the subshell scaling are discussed. In Sec. III the scaling procedures and scaled subshell ionization stopping powers are presented. In Sec. IV calculations of proton stopping power using

scaled subshell ionization stopping powers (with Herman and Skillman<sup>11</sup> atomic ionization energies) and explicit calculations of the contribution of excitation are compared with stopping-power measurements and other calculations across the periodic table at proton energies of 0.4, 1.0, 3.0, and 10.0 MeV, while Sec. V discusses in greater detail the stopping-power calculations for high- $Z$  elements

( $Z \geq 78$ ).

In Sec. VI relativistic effects are briefly discussed and it is argued that for the range of proton energies of interest here (up to 10 MeV) that relativistic effects play a negligible role in stopping power. In Sec. VII the relation of these explicit calculations to other stopping-power calculations is discussed. Conclusions are presented in Sec. VIII.

## II. MECHANICS OF THE CALCULATIONS

In the plane-wave Born approximation the proton stopping power is given by

$$S = \frac{-1}{n} \frac{dE}{dx} = \sum_{nl} S_{\text{ion}}^{nl} + S_{\text{ex}}^{nl} \quad (1a)$$

with  $n$  the target number density and

$$S_{\text{ion}}^{nl} = \frac{4\pi a_0^2}{(m_e/m_p)E_p} \int_0^{\epsilon_{\text{max}}} d\epsilon \int_{k_{\text{min}}^2}^{k_{\text{max}}^2} \sum_{l'=0}^{\infty} \frac{df_{nl}}{d\epsilon}(\epsilon, K^2, l') \frac{dK^2}{K^2}, \quad (1b)$$

$$S_{\text{ex}}^{nl} = \frac{4\pi a_0^2}{(m_e/m_p)E_p} \int_{K_{\text{min}}^2}^{K_{\text{max}}^2} \sum_{n'l'} f_{nl}(n'l', K^2) \frac{dK^2}{K^2}, \quad (1c)$$

where  $a_0$  is the Bohr radius,  $E_p$  is the proton energy in Ry, and  $(m_e/m_p)$  is the electron-to-proton mass ratio. For  $E_{nl}$ , the  $nl$  subshell ionization energy, with  $\Delta E = \epsilon + E_{nl}$  for ionization and  $\Delta E = E_{nl} - E_{n'l'}$  for excitation,

$$K_{\text{min}}^2 = \frac{m_p}{m_e} [\sqrt{(E_p)} \pm (E_p - \Delta E)^{1/2}]^2.$$

The generalized oscillator strength between initial orbital  $nl$  and final orbital  $\epsilon l'$  (ionization) and  $n'l'$  (excitation) is given by

$$\frac{df_{nl}}{d\epsilon}(\epsilon, K^2, l') = \frac{\Delta E}{K^2} |\langle nl | e^{i\vec{K} \cdot \vec{r}} | \epsilon l' \rangle|^2 \quad (2a)$$

for ionization and

$$f_{nl}(n'l', K^2) = \frac{\Delta E}{K^2} |\langle nl | e^{i\vec{K} \cdot \vec{r}} | n'l' \rangle|^2 \quad (2b)$$

for excitation, where all energies are in Ry, and  $K$  is in inverse Bohr radii. The generalized oscillator strengths (GOS's) were calculated by approximating  $[-rV(r)]$  of Herman and Skillman<sup>11</sup> by a series of straight lines. With this approximation the Schrödinger equation is exactly solvable in terms of Whittaker functions, permitting the rapid generation of continuum orbitals. The approximation is

discussed in earlier papers on electron and proton ionization cross sections.<sup>8,9</sup> For bound states the solution to the Schrödinger equation satisfying boundary conditions at zero and infinity leads to an eigenvalue equation. The eigenvalue equation was used to determine eigenvalues and eigenfunctions for both filled and empty bound states. The latter were used to calculate excitation GOS's, cross sections, and stopping power. Generally, we used 12 empty bound states, the three lowest-lying empty  $s$ ,  $p$ , and  $d$  orbitals, the two lowest-lying  $f$  orbitals, and the  $5g$  orbital. In calculating the excitation GOS the output was comparable in size to the ionization GOS; the computer time was an order of magnitude smaller for the excitation calculations because the final-state angular momentum is limited to one value per transition.

The data handling introduces an additional feature in the stopping-power calculations that was not present in the ionization-cross-section calculations. The ionization calculations were performed on a 20 by 25 grid of  $K^2/E_{nl}, \epsilon/E_{nl}$ . If, for some high value of  $\epsilon/E_{nl}$ , all the GOS values, except at the Bethe ridge, were more than six orders of magnitude smaller than the largest GOS value for the subshell, then the calculation was terminated. Typically this occurred for  $\epsilon/E_{nl} > 50$ . At  $\epsilon/E_n > 50$ , one is in regime where the Bethe ridge dominates the GOS, i.e.,

$$\sum_{l'} \frac{df}{d\epsilon}(\epsilon, K^2, l') \approx Z_{nl} \delta(\epsilon - K^2),$$

where the  $\delta$  function is used to represent the narrowly peaked Bethe ridge [to accurately calculate

$$\begin{aligned} & \frac{4\pi a_0^2}{(m_e/m_p)E_p} \int_{50E_{nl}}^{E_p - E_{nl}} d\epsilon \int_{K_{\min}^2}^{K_{\max}^2} Z_{nl} \delta(K^2 - \epsilon) \frac{dK^2}{K^2} \\ &= \frac{4\pi a_0^2}{(m_e/m_p)E_p} \int_{50E_{nl}}^{E_p - E_{nl}} Z_{nl} \frac{d\epsilon}{\epsilon} \theta \left[ \frac{m_p}{m_e} [\sqrt{E_p} + (E_p - E_{nl} - \epsilon)^{1/2}] - \epsilon \right] \\ & \times \theta \left[ \epsilon - \frac{m_p}{m_e} [\sqrt{E_p} - (E_p - E_{nl} - \epsilon)^{1/2}] \right]. \end{aligned} \quad (3)$$

The argument of the first  $\theta$  function ( $K_{\max}^2 - \epsilon$ ) decreases with increasing  $\epsilon$  and is positive at  $\epsilon = E_p - E_{nl}$ , and so does not affect the integral. The argument of the second  $\theta$  function ( $\epsilon - K_{\min}^2$ ) is positive if

$$E_p > \frac{1}{4} \frac{m_p}{m_e} \frac{[\epsilon(1 + m_e/m_p) + E_{nl}]^2}{\epsilon}.$$

For  $\epsilon > 50E_{nl}$  this is approximately  $E_p > 12.5(m_p/m_e)E_{nl}$ . Since these calculations are

the shape of the ridge is difficult as the number of  $l'$  values in the sum in Eq. (1b) increases rapidly with  $\epsilon$ ].

The contribution of this term to the stopping power is

done up to 10-MeV proton energy, the Bethe ridge for  $\epsilon/E_{nl} > 50$  will contribute to those subshells with ionization energies less than 435 eV. In practice it can be as much as a 20% correction at 10 MeV for the outermost subshell. For fixed proton energy the maximum  $\epsilon$  in Eq. (3) is  $\epsilon \approx 4E_p(m_e/m_p)$ , so the Bethe-ridge contribution is

$$\begin{aligned} & \frac{4\pi a_0^2 Z_{nl}}{(m_e/m_p)E_p} \theta(E_p - 12.5E_{nl}m_p/m_e) \\ & \times \ln(4E_p m_e / 50m_p E_{nl}). \end{aligned}$$

TABLE I. Parameters for the scaled 1s, 2s, and 2p proton subshell ionization stopping power;  $[(-1/n)(dE/dx)]_{nl} E_{nl}^{\alpha_{nl}} = g_i(m_e E_p / m_p E_{nl})$  with  $g_i$  in units of  $10^{-15}$  eV cm<sup>2</sup> Ry <sup>$\alpha$</sup> . The subscripts a–c refer to the following values of  $\alpha_{nl}$  and  $E_{nl}$ .

$\eta$	2s				2p		
	1s $\alpha = 1.00$	a: $0.9 \leq E_I \leq 3.2$ , $\alpha = 1.10$	b: $3.2 \leq E_I \leq 25$ , $\alpha = 0.80$	c: $E_I \geq 25$ , $\alpha = 1.00$	a: $0.4 \leq E_I \leq 1.3$ , $\alpha = 1.31$	b: $1.3 \leq E_I \leq 15$ , $\alpha = 0.74$	c: $E_I \geq 15$ , $\alpha = 1.00$
$g$	$g_a$	$g_b$	$g_c$	$g_a$	$g_b$	$g_c$	
0.10	0.53	0.83	0.32	0.40	1.5	1.10	2.0
0.15	1.20	1.41	0.75	1.15	2.6	1.95	3.9
0.20	1.90	1.96	1.20	2.05	3.6	2.85	5.9
0.30	3.35	2.90	2.00	3.80	5.4	4.45	9.5
0.50	5.60	4.30	3.20	6.50	8.2	7.00	15.5
0.70	7.20	5.30	3.90	8.15	10.2	8.90	20.3
1.00	8.70	6.20	4.50	9.20	12.4	10.9	24.5
1.50	9.30	7.00	4.75	9.30	14.4	13.0	27.2
2.0	9.30	6.80	4.65	8.75	15.5	13.9	27.5
3.0	9.10	6.40	4.30	7.50	16.0	13.9	26.0
5.0	7.90	5.40	3.50	5.90	14.8	12.9	21.5
7.0	6.80	4.55	2.90	4.80	13.5	11.8	18.5
10.0	5.70	3.65	2.30	3.85	11.8	10.2	15.0
15.0		2.75	1.73	2.85	9.5	8.3	11.8
20.0		2.20	1.40	2.35	8.0	7.0	9.6
30.0		1.60			6.1	5.35	
50.0		1.05			4.0	3.65	
70.0					3.0	2.80	
100.0					2.2	2.10	

TABLE II. Parameters for the scaled 3s, 3p, and 3d proton subshell ionization stopping power;  $[(-1/n)(dE/dx)]_{nl}E_{nl}^{\alpha_{nl}} = g_i(m_e E_p/M_p E_{nl})$  with  $g_i$  in units of  $10^{-15}$  eV cm<sup>2</sup> Ry <sup>$\alpha$</sup> . The subscripts a–d refer to the following values of  $\alpha_{nl}$  and  $E_{nl}$ .

$\eta$	3s			3p			3d			
	$g_a$	$g_b$	$g_c$	$g_a$	$g_b$	$g_c$	$g_a$	$g_b$	$g_c$	
0.10	0.83	0.22	0.34	3.1	4.6	0.90	1.50	2.3	1.60	3.8
0.15	1.90	0.58	1.08	6.2	7.5	1.85	3.45	3.3	2.60	6.8
0.20	3.00	0.99	2.03	9.2	10.2	2.85	5.85	4.2	3.45	9.8
0.30	4.8	1.78	3.90	14.0	14.8	4.65	10.8	5.8	4.95	15.2
0.50	7.6	2.95	6.85	21.2	21.2	7.30	18.2	8.0	6.15	23.5
0.70	9.2	3.60	8.40	25.5	25.4	9.20	22.8	9.5	8.5	30.5
1.00	10.2	4.00	9.35	28.5	28.2	10.9	26.8	11.2	9.8	37.0
1.50	10.2	3.95	9.00	29.2	30.0	12.2	27.8	12.4	11.3	43.0
2.0	9.5	3.75	8.20	28.2	29.2	12.5	26.5	13.2	12.1	46.0
3.0	7.9	3.35	6.90	25.6	27.0	11.5	23.5	14.0	13.0	44.0
5.0	6.1	2.55	5.15	20.8	22.5	10.5	18.5	14.2	13.0	38.0
7.0	4.9	2.10	4.05	17.5	18.8	8.10	15.5	14.0	12.8	33.5
10.0	3.8	1.65		14.0	15.3	6.50	12.2	13.5	11.9	27.5
15.0	2.75	1.24		10.8	12.6	5.00		12.9	10.3	21.0
20.0	2.15	0.98		8.8	9.4	4.10		11.8	9.0	
30.0	1.53	0.70		6.3	6.8	2.95		9.8	7.2	
50.0	0.98	0.46		4.15	4.6	1.93		7.4	5.0	
70.0				3.10	3.45	1.44		5.7	3.80	
100.0				2.28	2.55	1.07		4.2	2.80	
150.0								2.95		
200.0								2.30		
300.0								1.63		
500.0								1.03		

This correction was included in all the calculations of total stopping power.  $Z_{nl}$  was set equal to the number of electrons in the subshell, in the absence of an alternative choice. For  $\epsilon \leq 50E_{nl}$ , the explicit calculations determine the integrated subshell oscillator strengths.

In the stopping-power calculations the Bethe ridge contributes a term proportional to  $(\ln E_p)/E_p$ , i.e., similar in form to the total stopping power. To the ionization cross section for protons the Bethe ridge contributes a term of the form

$$\theta(E_p - 12.5E_{nl}m_p/m_e)(1/50E_{nl} - m_p/4m_e E_p)/E_p,$$

i.e., a term of the form  $1/E_p$ . Since the total ionization cross section is proportional to  $(\ln E_p)/E_p$ , the Bethe ridge does not contribute significantly to the ionization cross section.

### III. SCALING OF THE SUBSHELL IONIZATION STOPPING POWER

The ionization contribution to the proton stopping-power peaks at  $E_p = (4-8)(m_p/m_e)E_{nl}$ .

This is a proton energy less than the threshold for Bethe-ridge effects as discussed in Sec. II. Thus the scaling results do not include the Bethe ridge which is treated separately. As in scaling electron and proton ionization cross sections<sup>8,9</sup> we look for a scaling law of the form

$$\left[ \frac{-1}{n} \frac{dE}{dx} \right]_{nl} (E_{nl})^{\alpha_{nl}} = g_{nl}(\eta),$$

$$\eta = \frac{m_e E_p}{m_p E_{nl}},$$

where  $\alpha_{nl}$  is a constant over broad ranges of  $E_{nl}$  and is unity for  $E_{nl}$  sufficiently large.  $\alpha_{nl}$  is determined by plotting the maximum of  $[(-1/n)(dE/dx)]_{nl}E_{nl}$  vs  $E_{nl}$ .  $g_{nl}(\eta)$  is obtained from the calculated representative elements with  $E_{nl}$  in a common range.

Tables I to V list the subshell scaling parameter  $\alpha_{nl}$  and scaling functions  $g_{nl}(\eta)$  for all the subshells up to 5f. For the 6s subshell, the 5s subshell

TABLE III. Parameters for the scaled 4s and 4p proton subshell ionization stopping powers;  $[(-1/n)(dE/dx)]_{nl} E_{nl}^{\alpha_{nl}} = g_i (M_e E_p / M_p E_{nl})$  with  $g_i$  in units of  $10^{-15}$  eV cm<sup>2</sup> Ry <sup>$\alpha$</sup> . The subscripts a–f refer to the following values of  $\alpha_{nl}$  and  $E_{nl}$ .

$\eta$	4s				4p					
	$g_a$	$g_b$	$g_c$	$g_d$	$g_a$	$g_b$	$g_c$	$g_d$	$g_e$	$g_f$
0.10	0.42	0.65	0.14	0.42	5.3	2.3	2.60	4.80	0.92	1.30
0.15	1.14	2.10	0.36	1.14	10.7	5.0	5.40	9.60	1.90	4.30
0.20	3.02	3.65	0.62	3.02	15.8	8.0	8.00	14.2	2.95	7.50
0.30	4.20	6.50	1.12	4.20	25.0	13.4	12.8	22.3	4.90	13.0
0.50	7.70	10.2	1.84	7.00	38.5	22.0	19.0	33.0	7.80	20.0
0.70	9.60	11.8	2.26	8.50	48.0	28.0	23.0	39.0	9.60	24.2
1.00	10.6	12.2	2.50	9.35	57.0	33.5	26.0	42.0	11.2	27.5
1.50	10.1	11.6	2.45	9.10	65.0	36.0	25.5	42.0	11.3	28.0
2.0	8.9	10.5	2.32	8.45	65.0	34.7	23.5	40.0	10.8	25.4
3.0	7.1	8.6	2.02	7.10	59.0	31.5	20.5	35.5	9.40	21.3
5.0	5.1	6.4	1.58	5.50	48.0	25.6	16.0	27.7	7.40	16.2
7.0	4.0	5.2	1.29		40.0	20.8	13.2	22.9	6.10	
10.0	3.05	3.95	1.03		31.5	16.4	10.4	18.2	4.80	
15.0	2.17	2.90	0.77		23.5	12.3	7.70	14.0	3.60	
20.0	1.70	2.28			19.0	9.9	6.20	11.2	2.85	
30.0	1.17	1.60			13.5	7.2	4.40	8.2		
50.0	0.73	1.00			8.6	4.7	2.85	5.5		
70.0	0.530	0.73			6.6	3.50	2.18			
100.0	0.395	0.535			4.9	2.58	1.62			

parameters were found to be appropriate.

To illustrate the determination of  $g_{nl}(\eta)$ , in Fig. 1, the calculated 4d subshell stopping power in scaled variables is shown for  $Z=42$  and 52,  $Z=54$  and 66, and  $Z=70$  and 98. These elements have the highest and lowest ionization energy in the ranges a, b, and c in Table IV. The  $Z=42$  results are normalized to 10 electrons. The open circles are the values listed in Table IV. The largest difference (20–25%) between the values in Table IV for the 4d subshell and the extreme atoms occur for case (a), the scaled 4d ionization stopping power for  $E_{4d} < 4.6$  Ry. In this region the 4d subshells is in transition from a partially filled outer shell to a filled inner shell, and with increasing ionization energy the peak of the ionization stopping power shifts to lower  $\eta$  values.

In Fig. 2 detailed calculations are presented for the stopping power of Xe. The solid curves are obtained from the scaled subshell stopping powers in Tables I to V, with Herman and Skillman<sup>11</sup> eigenvalues, and with the Bethe-ridge correction. The open and solid circles are direct calculations for Xe

using model eigenvalues, and not including the Bethe-ridge correction. The diagonal slashes indicate the proton energy above which the Bethe-ridge correction is nonzero for the 5p, 5s, 4d, and 4p subshells. At 10 MeV the Bethe-ridge correction is about 20% for the 5p, 4d, and 4p subshells and 50% for the (negligible) 5s subshell.

The curve labeled total in Fig. 2 includes the explicitly calculated excitation contribution to stopping power. The experimental values of Reynolds *et al.*<sup>12</sup> (with error bars) and Chilton *et al.*<sup>13</sup> (open triangles) are also shown. The measurements of Chilton *et al.*<sup>13</sup> are in excellent agreement with the calculated total stopping power. Where they overlap, the measurements of Reynolds *et al.*<sup>12</sup> are 15% higher than the measurements of Chilton *et al.*<sup>13</sup> While the latter authors<sup>13</sup> point out the 15% discrepancy, they do not discuss it. Between 0.1 and 0.6 MeV the measurements of Reynolds *et al.* are 15% larger than the calculations.

Recent measurements by Besenbacher *et al.*<sup>14</sup> agree with the measurements of Reynolds *et al.*, and are 15% higher than the calculations. This is

TABLE IV. Parameters for the scaled  $4d$  and  $4f$  proton subshell ionization stopping powers;  $[(-1/n)(dE/dx)]_{nl} E_{nl}^{\alpha_{nl}} = g_i(m_e E_p/m_p E_{nl})$  with  $g_i$  in units of  $10^{-15}$  eV cm<sup>2</sup> Ry <sup>$\alpha$</sup> . The subscripts a–d refer to the following values of  $\alpha_{nl}$  and  $E_n$ .

$\eta$	$4d$				$4f$			
	$g_a$	$g_b$	$g_c$	$g_d$	$g_a$	$g_b$	$g_c$	$g_d$
	a: $0.6 \leq E_I \leq 4.6$ , b: $4.6 \leq E_I \leq 12.0$ , c: $12.0 \leq E_I \leq 100.0$ , d: $E_I \geq 100.0$ ,	$\alpha=0.68$ $\alpha=1.61$ $\alpha=0.74$ $\alpha=1.00$			a: $0.5 \leq E_I \leq 1.7$ , b: $1.7 \leq E_I \leq 14.0$ , c: $14.0 \leq E_I \leq 70.0$ , d: $E_I \geq 70.0$ ,	$\alpha=0.61$ $\alpha=0.61$ $\alpha=0.61$ $\alpha=1.00$		
0.10	3.6	16.0	1.30	3.15	2.8	1.78	1.35	6.5
0.15	5.8	26.5	2.32	6.20	4.0	2.70	2.05	10.0
0.20	8.0	36.0	3.30	9.50	5.0	3.45	2.75	13.4
0.30	11.7	53.0	5.10	16.0	6.5	4.70	3.95	19.5
0.50	17.0	78.0	7.80	26.5	8.5	6.50	5.80	29.5
0.70	20.4	96.0	9.80	34.0	9.8	7.60	7.20	37.5
1.00	23.7	113.0	11.9	42.0	11.0	8.70	8.60	47.0
1.50	26.7	123.0	13.5	46.5	11.6	9.80	10.2	56.5
2.0	27.8	123.0	14.0	46.0	12.0	10.6	11.1	62.0
3.0	27.2	118.0	13.4	42.5	12.0	11.3	12.0	65.5
5.0	25.0	103.0	11.7	34.5	12.0	12.0	12.0	61.5
7.0	22.5	90.0	10.0	28.5	12.0	12.0	11.3	55.0
10.0	19.8	73.0	8.3		11.8	11.8	10.0	46.0
15.0	16.0	57.5	6.6		11.4	10.7	8.4	
20.0	13.5	47.0	5.4		11.2	9.8	7.2	
30.0	10.3	35.5	3.9		10.6	8.4	5.5	
50.0	6.9	24.0			9.4	6.5		
70.0	5.2	18.4			8.4	5.3		
100.0	3.7	13.8			7.3	4.2		
150.0	2.75				5.9	3.1		
200.0	2.20				5.0			
300.0	1.63				3.8			
400.0					3.1			

somewhat surprising. In Ref. 9 my calculated Xe proton ionization cross section is in excellent agreement with the measured total cross section of Toburen,<sup>15</sup> though Toburen's error bars are larger than 15%.

From Fig. 2 it is clear that the total stopping power, even at 10 MeV, results from a complex combination of individual subshell stopping powers. At 10 MeV the  $4d$  subshell, containing 19% of the electrons in Xe, contributes 34% of the stopping power; the  $5p$  subshell with 11% of the Xe electrons contributes 20% of the stopping power. This strongly suggests for ions that removal of the outer electrons will result in a significant decrease in stopping power for protons with less than 10 MeV energy.

In the following section my explicit calculations are compared with measurements made across the periodic table, principally on solids. The difference between the calculations and the measurements on solids is never more than 15%, never more than the

difference between the calculations and the measurements on Xe. That the difference is this small, even though subshell ionization thresholds in solids are considerably different than in atoms is a consequence of (1) dominance of ionization in stopping power, (2) the applicability to solids of the subshell scaling law, and (3) the form of the subshell scaling. That is, if

$$\left[ \frac{-1}{n} \frac{dE}{dx} \right]_{nl} = \frac{1}{E_{nl}^{\alpha_{nl}}} g_{nl}(\eta)$$

and

$$g_{nl}(\eta) = (A/\eta) \ln(\beta\eta)$$

then with  $\eta = (M_e/M_p)E_p/E_{nl}$

$$\left[ \frac{-1}{n} \frac{dE}{dx} \right]_{nl} = A \frac{M_p}{M_e} \frac{1}{E_p} \left[ \frac{1}{E_{nl}} \right]^{\alpha_{nl}-1} \ln \left[ \beta \frac{M_e}{M_p} \frac{E_p}{E_{nl}} \right].$$

But over wide energy ranges  $\alpha_{nl}$  is unity or close to

TABLE V. Parameters for the scaled 5s, 5p, 5d, and 5f proton subshell ionization stopping powers;  $[(-1/n)(dE/dx)]_{nl}E_{nl}^{\alpha_{nl}} = g_i(m_e E_p/m_p E_{nl})$  with  $g_i$  in units of  $10^{-15}$  eV cm<sup>2</sup> Ry <sup>$\alpha$</sup> . The subscripts a–c refer to the following values of  $\alpha_{nl}$  and  $E_{nl}$ .

$\eta$	5s		5p			5d		5f
	$g_a$	$g_b$	a: $0.4 \leq E_I \leq 1.65$ , b: $1.65 \leq E_I \leq 10$ , c: $10 \leq E_I \leq 21$ ,	$\alpha = 1.16$ $\alpha = 0.885$ $\alpha = 1.41$	$g_c$	a: $0.8 \leq E_I \leq 3.8$ , b: $3.8 \leq E_I \leq 11$ ,	$\alpha = 0.58$ $\alpha = 1.40$	a: $0.9 < E_I \leq 2.0$ $\alpha = 0.80$
0.10	0.18	0.56	0.75	0.86	4.0	2.60	8.0	2.19
0.15	0.72	2.35	2.1	2.40	11.0	4.45	15.0	3.30
0.20	1.65	4.90	4.00	4.35	19.0	6.3	22.0	4.35
0.30	3.95	10.3	7.65	8.4	35.0	9.8	35.0	6.0
0.50	7.85	17.2	14.3	15.2	60.0	15.3	56.0	8.7
0.70	9.35	19.0	19.8	20.0	72.5	19.5	71.0	10.9
1.00	9.80	18.6	25.4	23.8	78.0	24.0	87.0	13.4
1.50	9.15	16.5	28.0	25.0	75.0	28.2	95.0	16.3
2.0	7.90	14.2	27.6	23.8	68.0	30.1	97.0	18.2
3.0	6.30	11.6	25.0	20.2	55.5	30.3	89.0	21.6
5.0	4.40	8.30	20.0	15.2	41.0	28.2	71.0	22.3
7.0	3.45	6.65	16.5	12.2	32.5	25.5	59.0	22.8
10.0	2.55	5.10	13.2	9.25	25.5	22.0	47.5	22.1
15.0	1.82	3.75	9.80	6.8	18.5	17.5	36.0	19.8
20.0	1.42	3.05	6.90	5.4	14.6	14.7	29.0	17.7
30.0	0.98	2.20	5.60	3.80	10.5	11.2	21.0	14.6
50.0	0.60		3.60	2.40	6.8	7.5	13.8	10.8
70.0	0.45		2.65	1.78		5.75	10.3	8.7
100.0	0.33		1.93	1.31		4.20	7.5	6.8
150.0						3.05		4.8
200.0						2.45		3.75
300.0								2.70

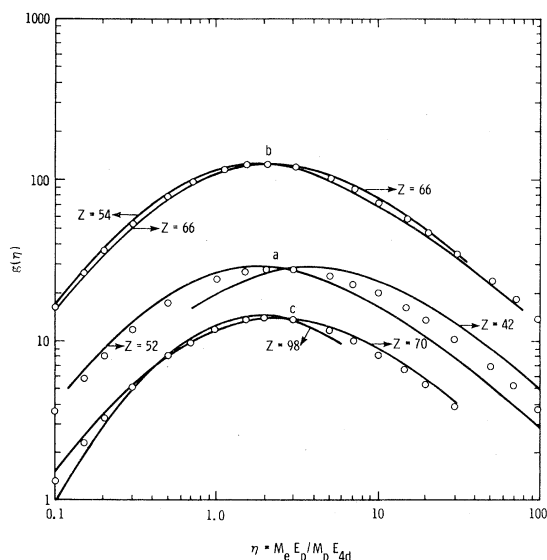


FIG. 1. Calculated  $g(\eta) = (-1/n)(dE/dx)(E_{4d})^{\alpha_{4d}}$  vs  $\eta = m_e E_p/m_p E_{4d}$  for  $Z=42$  and  $52$ ,  $Z=54$  and  $66$ , and  $Z=70$  and  $98$ .

it, so the change in subshell stopping power with ionization threshold is expected to be small.

#### IV. COMPARISON WITH EXPERIMENTAL STOPPING-POWER MEASUREMENTS

As mentioned in the Introduction, as yet subshell scaling laws for excitation cross sections (or, effectively, excitation stopping powers) have not been found. Extensive calculations of atomic excitation GOS's have been done, i.e., for all  $Z$  up to 11, for  $12 \leq Z \leq 54$  in steps of 2, and for  $54 \leq Z \leq 94$  in steps of 4, and for  $Z=79, 80, 84$ , and  $88$ . However, not all subshells in each of these elements is included. With these explicit excitation GOS's excitation cross sections and contribution to proton stopping power can be calculated, using the model eigenvalues. In conjunction with the scaled subshell ionization stopping powers in Tables I–V, the total stopping power can be calculated and compared

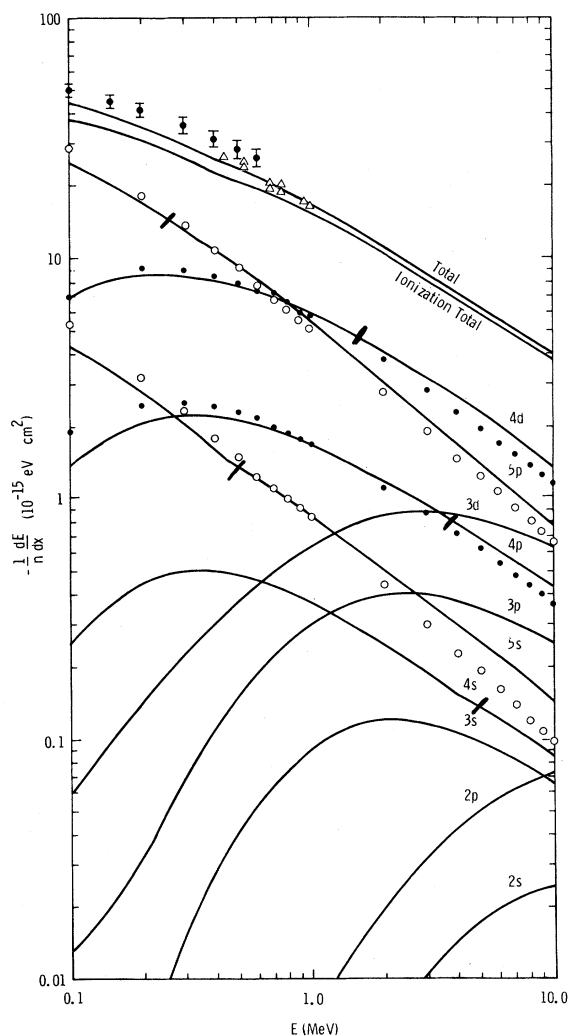


FIG. 2. Contributions of subshell ionization (solid lines from scaling, open and solid circles from direct calculations) and excitation to total proton stopping power of Xe. The diagonal slashes indicate the boundary of  $E_p = 12.5m_p E_{nl}/m_e$ . The experimental data are from Ref. 12 (with error bars) and Ref. 13 (triangles).

with experiment, assessing the validity of this approach. The calculations enable one to compare the relative importance of ionization and excitation across the periodic table, and indicate regions in  $Z$  where additional stopping-power measurements would be useful. The calculations are shown in Figs. 3–5.

The experimental stopping-power values are discussed in the invaluable compilation and critical evaluation of Andersen and Ziegler.<sup>16</sup> Most of the experimental data were obtained from measurements on solids and there will be some disagreement

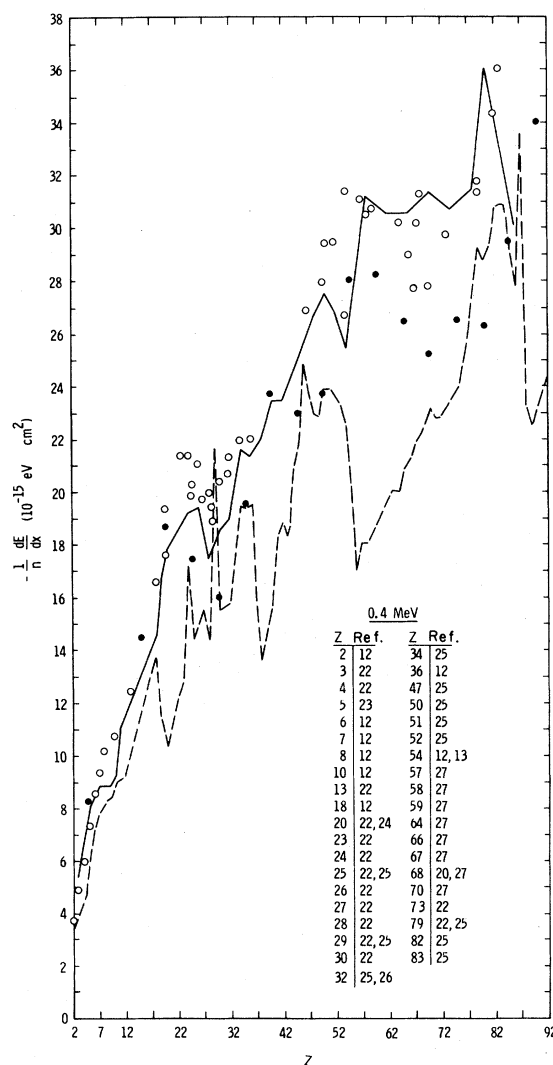


FIG. 3. Calculated total proton stopping power (solid curve) and its ionization component (dashed curve) at 0.4 MeV. The open circles are experimental data and the solid circles are the theoretical values of Ref. 17.

between the calculated atomic stopping power and the measured solid stopping power. However, the disagreement is generally no more than 15%, and as pointed out in Sec. III a 15% discrepancy exists between the calculations and the most recent measurements on Xe.<sup>14</sup>

In Figs. 3–5 the dashed curve is the contribution of ionization to the proton stopping power, while the solid curve includes both excitation and ionization. The open circles are experimental measurements. In Figs. 3 and 4 the solid circles are total proton stopping power calculated by Chu and Powers<sup>17</sup> using an approximate dielectric function

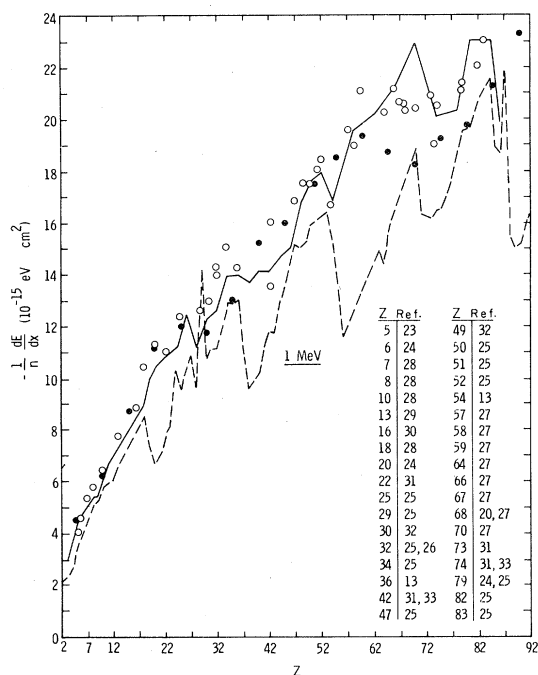


FIG. 4. Calculated total proton stopping power (solid curve) and its ionization component (dashed curve) at 1 MeV. The open circles are experimental data and the solid circles are the theoretical values of Ref. 17.

formalism with the medium treated as a nonuniform electron gas.<sup>18</sup> In Fig. 5 the solid circles are the Bethe formula<sup>6</sup> with the  $I/Z$  values calculated by Chu and Powers<sup>19</sup> using a modification of the statistical approach of Lindhard and Scharff.<sup>5</sup>

My calculated ionization stopping power shows sharp peaks at  $Z=24$  and  $Z=29$ , arising from use of the configuration  $(3d)^n(4s)^1$  rather than  $(3d)^{n-1}(4s)^2$  as the ground state for these elements. The Herman and Skillman<sup>11</sup> eigenvalues for the  $3d$  electron in these configurations are considerably lower (0.743 Ry at  $Z=29$ ) than the other first transition row elements (1.16 Ry at  $Z=28$  and 1.26 Ry at  $Z=30$ ), consequently the  $3d$  subshell stopping power is higher. This sensitivity of the stopping power to outer-shell ionization energy is consistent with the observation<sup>20</sup> of 10–15% departures from the Bragg additivity rule.<sup>21</sup> The peak at  $Z=29$  is even more striking as excitation calculations were not done at  $Z=29$ , and the total stopping power at  $Z=29$  which is an interpolation between  $Z=28$  and 30 is lower than the ionization contribution to the stopping power at  $Z=29$ , which was calculated explicitly.

The ionization calculations, particularly in Fig. 3, show large peaks at  $Z=18, 34$  to  $36, 46$  and  $82$  to  $84$ , corresponding to filling of the  $3p, 4p, 4d$ , and  $5d$

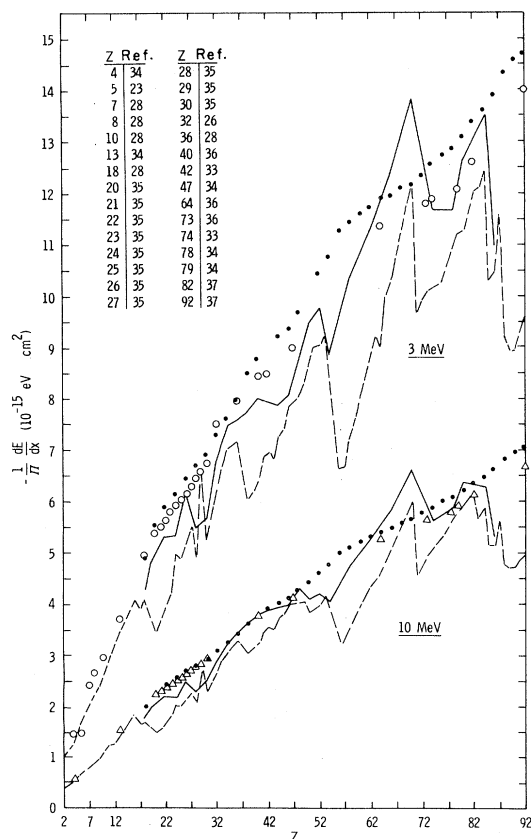


FIG. 5. Calculated total proton stopping power (solid curve) and its ionization component (dashed curve) at 3 and 10 MeV. The open circles and triangles are experimental data while the dotted curve is the Bethe formula with the  $I/Z$  values of Ref. 19.

subshells. The excitation contribution is large for  $19 \leq Z \leq 30$ ,  $37 \leq Z \leq 45$ , and for  $Z > 54$ . For  $19 \leq Z \leq 30$  the excitation contribution to the stopping power is dominated by the  $(3p)^6(3d)^n - (3p)^5(3d)^{n+1}$  transition. The  $Z=26$  calculations included excitation of the  $3p, 3d$ , and  $4s$  subshells, while for  $Z=24$  and  $28$  only the  $3d$  and  $4s$  subshells were treated. At  $Z=26$  the calculations are in excellent agreement with the measurements at all proton energies shown while for  $Z=24$  and  $28$ , the calculations are slightly below the measurements. For  $37 \leq Z \leq 45$  the  $4p-4d$  transition dominates the excitation contribution to stopping power. For  $54 \leq Z \leq 70$  the  $5p-5d$  and  $4d-4f$  transitions are comparable and dominate the excitation contribution to stopping power. Above  $Z=70$  the  $5p-5d$  transition is dominant.

The recent measurements of Knudsen *et al.*<sup>27</sup> on the rare earths are in excellent agreement with the calculations at 400 keV for  $Z=57, 58, 59, 64$ , and

68, while at  $Z=67$  and  $70$ , the measurements are 10% lower than the calculations. At 1 MeV there is excellent agreement between the measurements at  $Z=57, 58, 64,$  and  $66$ , while the measurements at  $Z=68$  and  $70$  lie below the calculated peak in the stopping power at  $Z=70$ . This peak is due to the complete filling of the  $4f$  subshell.

The structure in my proton stopping power vs  $Z$  curves is not new. It is apparent from the data and the calculations of Chu and Powers shown in Figs. 3 and 4. The differences among the data, the two calculations of Chu and Powers, and my calculations are less than 20% at 0.4 MeV and less than that at higher energies. However, as shown in Fig. 2 for high- $Z$  elements the stopping power for protons of less than 10 MeV energy is dominated by the outer subshells whose ionization energies satisfy the assumptions in the Bethe treatment.

## V. THE STOPPING POWER OF HIGH-Z ATOMS

The following paper presents calculations on the proton stopping power of gold ions. For some ions the explicit calculations of total stopping power are significantly different than the results obtained with the scaling procedure, principally due to the high-energy behavior of the  $5d$  subshell stopping power. The subshell stopping power at high energy is dominated by the optical oscillator strength and one is tempted to associate the aforesaid differences with anomalies in the  $5d$  optical oscillator strengths. The one-electron central field photoionization calculations of Combet-Farnoux<sup>38</sup> (which are reproduced in my one-electron GOS calculations) show an anomalous behavior for the  $5d$  cross sections as a function of  $Z$  with  $79 \leq Z \leq 86$ . The calculated  $5d$  photoionization cross section has a maximum above the ionization threshold, and the value of the maximum increases at  $Z=86$ . Combet-Farnoux<sup>39</sup> later shows that interchannel interaction broadens these maxima.

The surprising feature of the scaled neutral-atom calculations is that this anomalous behavior of the  $5d$  photoionization cross section *does not* affect the scaled stopping power. In Fig. 6  $g(\eta)$  vs  $\eta$  for the  $5d$  subshells is shown for regions (a) and (b) of Table V.  $Z=86$  is the highest- $Z$  element in region (a) and the lowest- $Z$  element in region (b). The open circles are the values listed in Table V. Figure 6 is comparable to Fig. 1 for the  $4d$  subshell. In region (b) the difference between the scaling function and the explicit calculations at  $Z=86$  and  $Z=102$  is no more than 10%. The open triangles and solid

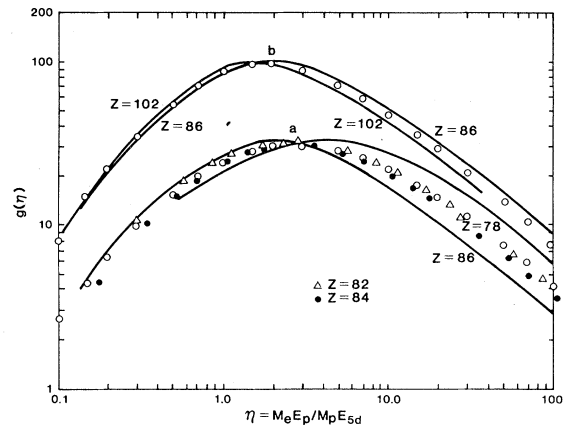


FIG. 6. Calculated  $g(\eta) = (-1/n)(dE/dx)(E_{5d})^{\alpha_{5d}}$  vs  $\eta = m_e E_p / m_p E_{5d}$  for  $Z=78$  and  $86$ , and  $Z=86$  and  $102$  (solid lines). The open circles are the interpolated values of Table V, while the triangles and solid circles are  $g(\eta)$  obtained from explicit calculations at  $Z=82$  and  $84$ .

circles are  $g(\eta)$  values obtained from explicit calculations at  $Z=82$  and  $Z=84$ , and are in excellent agreement with  $g(\eta)$  of Table V. While there are

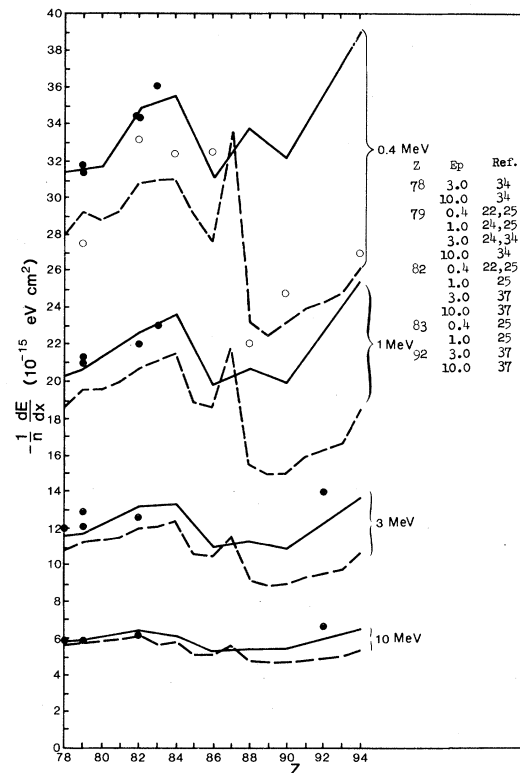


FIG. 7. Calculated total proton stopping power (solid line) and its ionization component (dashed line) for  $78 \leq Z \leq 94$ . The open circles are the explicit calculation of the ionization component at 0.4 MeV. The solid circles are experimental measurements.

variations of as much as 40% between the  $g(\eta)$  values of Table V and the explicit calculations at  $Z=78$  and  $Z=86$ , the variation is due to an overall shift of the maximum and not due to the anomaly in the  $5d$  oscillator strength.

Finally in Fig. 7 the calculated ionization (dashed line) and total-stopping-power calculations are shown for  $78 \leq Z \leq 94$  at 0.4, 1.0, 3.0, and 10 MeV. At 0.4 MeV the results of explicit ionization calculations including all subshells from the  $4f$  to  $7s$  are shown as open circles. They differ by no more than 10% from the results (dashed lines) calculated with the scaling laws. Thus the 40% variation in the scaled  $5d$ , stopping power does not strongly influence the total-stopping-power calculation. Except at  $Z=92$  the calculated total stopping power is in excellent (better than 10%) agreement with the measurements. At  $Z=92$  the disagreement is on the order of 10–15% but the calculations are merely an interpolation between calculations at  $Z=90$  and  $Z=94$ .

## VI. RELATIVISTIC EFFECTS

The GOS calculations in this and the following paper are nonrelativistic. For 10-MeV protons the relativistic correction is on the order of 1 to 2%. In Ref. 9 comparison is made between nonrelativistic proton ionization cross sections for the  $2s$  and  $2p$  subshells calculated with the GOS used in these stopping-power calculations and measurements by Barros Leite *et al.*<sup>40</sup> on uranium ( $Z=92$ ). The agreement between the calculations and experiment is good, indicating no significant distortion due to the nonrelativistic treatment of the  $2s$  and  $2p$  subshells. On the other hand, in comparing the calculated  $1s$  cross section with the measurements of Jarvis *et al.*<sup>41</sup> for 160-MeV incident protons (in Ref. 9), significant differences are seen for Pb and U targets, and the difference is attributed to the neglect of relativity in the  $1s$  orbital. However, as Fig. 2 shows, the  $1s$  (and  $2s$  and  $2p$ ) subshells contribute a negligible fraction of the total stopping power of Xe for protons of 10 MeV or less energy.

Further, to the extent that relativistic effects can be incorporated into a nonrelativistic calculation either by using an unmodified nonrelativistic orbital and a relativistic energy correction (as is often done in treating inner-shell spin-orbit splitting) or by using a nonrelativistic energy orbital rescaled to the relativistic energy value and a relativistic correction (as is often done with scaled hydrogenic orbitals for inner-shell orbitals), then, in the region of classical

scaling, relativistic corrections are a second-order effect. As a simple example consider six  $2p$  electrons with ionization energy  $E_0$ . Spin-orbit interaction splits the six  $2p$  electrons into two  $2p_{1/2}$  electrons with ionization energy  $E_0 + 2\Delta E_0$  and four  $2p_{3/2}$  electrons with ionization energy  $E_0 - \Delta E_0$ . In the nonrelativistic calculation, in the classical scaling region, the  $2p$  subshell stopping power is  $S_{2p}^{\text{NR}} = g_{2p}(E_p/E_0)/E_0$ . If one assumes that the relativistic effects can be treated as an energy rescaling so that the stopping power in the relativistic case  $S_{2p}^{\text{R}}$ , can be written as

$$S_{2p}^{\text{R}} = \frac{2}{6}g_{2p}(E_p/E_0 + 2\Delta E_0)/(E_0 + 2\Delta E_0) + \frac{4}{6}g_{2p}(E_p/E_0 - \Delta E_0)/(E_0 - \Delta E_0),$$

then expansion of  $S_{2p}^{\text{R}}$  in  $\Delta E_0/E_0$  shows that

$$S_{2p}^{\text{R}} = S_{2p}^{\text{NR}} + O((\Delta E_0/E_0)^2).$$

Thus for stopping power the relativistic correction for spin-orbit splitting is second order in the relativistic effect, while for ionization (where classical scaling has a  $1/E_0^2$  dependence) the correction is first order.

In summary, the proton ionization calculations indicate a significant effect on the  $1s$  cross section for Pb and U, attributable to relativistic distortion of the  $1s$  orbital. However, the  $1s$  subshell contributes a negligible fraction of the stopping power of high- $Z$  materials for protons with less than 10 MeV energy. For the  $2s$  and  $2p$  subshells no significant relativistic effect was found at proton energies where the ionization cross section is large. Finally, by the argument given above, stopping power is less sensitive than ionization cross sections to relativistic distortion of inner-shell orbitals.

My conclusion is that in this and the following paper there are no significant neglected relativistic effects.

## VII. RELATION TO OTHER APPROACHES

As alternatives to the explicit plane-wave Born-approximation calculations done here, proton stopping power can be calculated by the modified free-electron gas dielectric response function of Lindhard and Scharff<sup>5</sup> or the Bethe theory with shell corrections. Besenbacher *et al.*<sup>14</sup> have recently reviewed the Lindhard-Scharff theory, pointing out that in the original theory there is a factor  $\gamma$  which was chosen to equal  $\sqrt{2}$ . They further point out that recent calculations of Inokuti *et al.*<sup>42</sup> on the Bethe mean excitation energy  $I$  for neutral atoms

suggests a somewhat smaller value for  $\gamma$ . However, Peek<sup>43</sup> has shown that with a constant  $\gamma$  the modified free-electron gas model predicts the wrong  $I$  value for hydrogenic ions, i.e., it predicts  $I\alpha Z^{3/2}$  where  $Z$  is the nuclear charge, when the proper limit is  $I\alpha Z^2$ . Thus the modified free-electron gas model appears to be of dubious validity for studying the proton stopping power of high- $Z$  ions.

The Bethe theory with corrections is equivalent to the plane-wave Born approximation used here. However, since the Bethe mean excitation energy  $I$  is obtained by summing over all subshells, and is accurate at very high proton energy where the corrections are small, the implication is that at low energy (10 MeV for high- $Z$  atoms or ions) the inner-shell corrections are not small. For example, Fig. 2 for Xe suggests that between 0.1 and 1.0 MeV the  $1s-4s$  subshells contribute negligibly to the proton stopping power, yet these 30 electrons contribute significantly to the mean excitation energy  $I$ . Thus, one expects these inner shells to provide a significant contribution to the correction term. To calculate the correction term for inner shells one needs the inner-shell GOS, not merely the inner-shell optical oscillator strength. One needs to calculate the GOS for subshells that contribute negligibly to the stopping power in our range of interest. It was decided that this was a poor research strategy. A reasonable research strategy was adopted; if the outer subshells dominate the stopping power then the outer-shell GOS should be calculated with the inner shells treated as a correction via scaling laws. If complete sets of subshells GOS's were obtained then the explicit Born calculations and the Bethe theory with shell corrections should produce the same result. But while the Bethe theory with corrections requires a complete set of subshell GOS's, the explicit Born calculations need only a limited set of explicit GOS's.

Alternatively, one may use the explicit Born-approximation results to estimate inner-shell corrections, i.e., by subtracting from the explicit results the Bethe asymptotic expression

$$-\frac{1}{n} \frac{dE}{dx} = \frac{4\pi a_0 2Z_e}{(M_e/M_p)E_p} \ln \left( \frac{4M_e E_p}{M_p I} \right)$$

providing an accurate  $I$  value is available.

### VIII. CONCLUSION

In this paper I have shown that the proton stopping power of neutral atoms can be calculated directly on a subshell by subshell basis, and that the ionization contribution to subshell stopping power can be written in a scaled form. The calculations for proton energies of less than 10 MeV show that outer subshells dominate the ionization stopping power, and that for atoms with partially filled shells excitation of the resonance transition to the partially filled shells contributes significantly to the stopping power. A surprising feature is the slow decrease in peak stopping power of the  $4f$  subshell with increasing ionization energy. The stopping powers calculated here are in good agreement with measured values, as are other calculations. This suggests the relative insensitivity of neutral-atom stopping power to the details of the calculation. The dominance of the stopping power by outer subshells suggests that there will be significant changes in stopping power with degree of ionization. The differences between these calculations and experiment (mostly on solids) is never more than 15% above 400 keV (above which energy one expects the plane-wave Born approximation to be accurate). Born calculations on electron and proton ionization cross sections are usually accurate to 20–25%, and the somewhat better accuracy in stopping-power calculations may be merely a result of cancellation of errors.

### ACKNOWLEDGMENT

This work was supported by the U. S. Department of Energy.

<sup>1</sup>E. Nardi, E. Peleg, and Z. Zinamon, *Phys. Fluids* **21**, 574 (1978).

<sup>2</sup>T. Mehlhorn, *J. Appl. Phys.* **52**, 6522 (1981), and private communication.

<sup>3</sup>Y. Hahn, *Phys. Rev. A* **18**, 1028 (1978).

<sup>4</sup>O. B. Firsov, *Zh. Eksp. Teor. Fiz.* **36**, 1517 (1959) [*Sov. Phys.—JETP* **9**, 1076 (1959)].

<sup>5</sup>J. Lindhard and M. Scharff, *K. Dan. Vidensk. Selsk.*

*Mat. Fys. Medd.* **27**, No. 15 (1953).

<sup>6</sup>H. A. Bethe, *Ann. Phys. (Leipzig)* **5**, 325 (1930); *Z. Phys.* **76**, 293 (1932).

<sup>7</sup>J. L. Dehmer, M. Inokuti, and R. P. Saxon, *Phys. Rev. A* **12**, 102 (1975).

<sup>8</sup>E. J. McGuire, *Phys. Rev. A* **16**, 73 (1977); **20**, 445 (1979).

<sup>9</sup>E. J. McGuire, *Phys. Rev. A* **22**, 868 (1980).

- <sup>10</sup>E. J. McGuire, following paper, Phys. Rev. A 26, 1871 (1982).
- <sup>11</sup>F. Herman and S. Skillman, *Atomic Structure Calculations* (Prentice-Hall, Englewood Cliffs, New Jersey, 1963).
- <sup>12</sup>H. K. Reynolds, D. N. F. Dunbar, W. A. Wenzel, and W. Whaling, Phys. Rev. 92, 742 (1953).
- <sup>13</sup>A. B. Chilton, J. N. Cooper, and J. C. Harris, Phys. Rev. 93, 413 (1954).
- <sup>14</sup>F. Besenbacher, H. H. Andersen, P. Hvelplund, and H. Knutsen, K. Dan. Vidensk. Selsk. Mat. Fys. Medd. 40, No. 3 (1979).
- <sup>15</sup>L. H. Toburen, Phys. Rev. A 9, 2505 (1975).
- <sup>16</sup>H. H. Andersen and J. F. Ziegler, *Hydrogen Stopping Power and Ranges in All Elements* (Pergamon, New York, 1977).
- <sup>17</sup>W. K. Chu and D. Powers, Phys. Lett. 38A, 267 (1972).
- <sup>18</sup>C. C. Rousseau, W. K. Chu, and D. Powers, Phys. Rev. A 4, 1066 (1971).
- <sup>19</sup>W. K. Chu and D. Powers, Phys. Lett. 40A, 23 (1972).
- <sup>20</sup>R. A. Langley and R. S. Blewer, Nucl. Instrum. Methods 132, 109 (1976).
- <sup>21</sup>W. H. Bragg and R. Kleeman, Philos. Mag. 10, 318 (1905).
- <sup>22</sup>M. Bader, R. E. Pixley, F. S. Mozer, and W. Whaling, Phys. Rev. 103, 32 (1956).
- <sup>23</sup>J. C. Overley and W. Whaling, Phys. Rev. 128, 315 (1962).
- <sup>24</sup>S. Gorodetzky, A. Chevallier, A. Pape, J. C. Sens, A. M. Bergdolt, M. Bres, and R. Armbruster, Nucl. Phys. A91, 133 (1967).
- <sup>25</sup>D. W. Green, J. W. Cooper, and J. C. Harris, Phys. Rev. 98, 466 (1955).
- <sup>26</sup>S. Gorodetzky, A. Pape, E. L. Cooperman, A. Chevallier, J. C. Sens, and R. Armbruster, Nucl. Instrum. Methods 70, 11 (1969).
- <sup>27</sup>H. Knudsen, H. H. Andersen, and V. Martini, Nucl. Instrum. Methods 168, 41 (1980).
- <sup>28</sup>J. B. Swint, R. M. Prior, and J. J. Ramirez, Nucl. Instrum. Methods 80, 134 (1970).
- <sup>29</sup>D. Kahn, Phys. Rev. 90, 503 (1953).
- <sup>30</sup>R. H. Langley, Phys. Rev. B 12, 3575 (1975).
- <sup>31</sup>E. Leminen, Ann. Acad. Sci. Fenn. Ser. AVI Phys., No. 386 (1972).
- <sup>32</sup>E. Leminen, A. Fontell, and M. Bister, Ann. Acad. Sci. Fenn. Ser. A6, No. 281 (1968).
- <sup>33</sup>E. I. Sirotinen, A. F. Tulinov, A. Fiderkevich, and K. S. Shyshkin, Radiat. Eff. 15, 149 (1972).
- <sup>34</sup>H. H. Andersen, C. C. Hanke, H. Sorensen, and P. Vajda, Phys. Rev. 153, 338 (1967).
- <sup>35</sup>H. H. Andersen, C. C. Hanke, H. Simonsen, H. Sorensen, and P. Vajda, Phys. Rev. 175, 389 (1968).
- <sup>36</sup>H. H. Andersen, H. Simonsen, H. Sorensen, and P. Vajda, Phys. Rev. 186, 372 (1969).
- <sup>37</sup>H. Sorensen and H. H. Andersen, Phys. Rev. B 8, 1854 (1973).
- <sup>38</sup>F. Combet-Farnoux, J. Phys. (Paris) 30, 521 (1969).
- <sup>39</sup>F. Combet-Farnoux, *Abstracts of Papers, Seventh IC-PEAC, Amsterdam, 1971*, edited by L. Branscomb *et al.* (North-Holland, Amsterdam, 1971).
- <sup>40</sup>C. V. Barros Leite, N. V. de Castro Faria, and A. G. de Pinho, Phys. Rev. A 15, 943 (1977).
- <sup>41</sup>O. N. Jarvis, C. Whitehead, and M. Shah, Phys. Rev. A 5, 1198 (1972).
- <sup>42</sup>M. Inokuti, T. Baer, and J. L. Dehmer, Phys. Rev. A 17, 1229 (1978).
- <sup>43</sup>J. M. Peek, Phys. Rev. A 26, 1030 (1982).